Nuclear Inst. and Methods in Physics Research, A 940 (2019) 50–55

Contents lists available at ScienceDirect

Nuclear Inst. and Methods in Physics Research, A

journal homepage: www.elsevier.com/locate/nima

Performance of four digital algorithms for $\gamma - \gamma$ timing with $LaBr_3$(Ce) scintillators

G. Simpson *, S. Curtoni, D. Dauvergne, M.-L. Gallin-Martel, S. Marcatilli, G. Thiamova

LPSC, Université Grenoble Alpes, CNRS/IN2P3, Institut National Polytechnique de Grenoble, F-38026 Grenoble Cedex, France

A R T I C L E I N F O

Keywords:
Fast timing
Digital timing algorithms
$LaBr_3$(Ce)
Time resolution

A B S T R A C T

Time resolution measurements were performed using four digital timing algorithms and a pair of truncated-cone shaped, 38-mm diameter $LaBr_3$(Ce) fast-timing scintillator detectors. The best resolution [FWHM=143(3) ps] was found for transitions from a ^{60}Co source when fitting the rising part of sampled waveforms with a cubic polynomial and applying a leading-edge threshold. An average-pulse autocovariance function performed slightly worse [155(3) ps], but was found to be better than digital constant-fraction [178(4) ps] and leading-edge [177(4) ps] algorithms. Use of a ^{152}Eu source allowed the performance of the four algorithms to be tested across a range of γ-ray energies with the $LaBr_3$(Ce) detectors. Here the autocovariance algorithm performed best. Changing the sampling speed showed minimal degradation in the time resolution at 20 GS/s, though at 4 GS/s the resolutions were 30–60% worse. These results show that at sampling speeds of 20 or 40 GS/s the time resolutions obtained are close to those reported for analogue pulse-processing electronics. Compared to other works, using slower sampling speeds but higher vertical resolution, slightly worse performance was obtained.

1. Introduction

Fast scintillator detectors are used for $\gamma - \gamma$ timing and have a wide range of applications, including lifetime measurements of excited nuclear states [1], medical positron-emission tomography (PET) and range monitoring in hadron therapy [2]. These scintillation crystals have the properties of modest energy resolution and fast decay times (ns), and are constructed often with the aim of optimizing the time rather than energy resolution of the system. Recent progress in the fabrication of lanthanide-halide crystals, such as $LaBr_3$(Ce), with an energy resolution of ~3% at 662 keV and time resolution as good as 98(2) ps for ~1.2 MeV photons [3] has given renewed interest in the use and development scintillator detectors, resulting in, for example, the construction of the FATIMA array [4,5]. The decay time of $LaBr_3$(Ce) is 16 ns and 63,000 photons are emitted per MeV of energy absorbed. This compares with a decay time of 0.7 ns and 1800 photons/MeV for the fast component of the commonly used BaF_2. These scintillator detectors can be used to measure nuclear-state lifetimes in the 10s-of-ps-to-ns time range [1,6,7]. To date analogue signal processing chains have been almost exclusively used in applications which require the very best time resolution.

In principle digital acquisition systems, with very high-speed sampling, should allow equivalent, or even improved, timing performance over analogue ones, as signal processing can reduce jitter and fixed-frequency noise and bespoke algorithms can be developed for a particular detection system. Recently, time resolutions approaching, and matching, the best ones achieved with analogue electronics have been obtained with $LaBr_3$(Ce) detectors, using digitizers with sampling frequencies of 0.5, 4 and 5 GS/s by applying digital timing algorithms [8–10]. An improved time resolution over analogue systems was earlier obtained with Ge detectors using digital pulse-shape analysis [11]. Furthermore, digital acquisition systems have other advantages over analogue ones including (potentially) lower cost per channel, fewer modules and timing stamping of individual hits, allowing offline event reconstruction. Any algorithms used for pulse-shape analysis should ideally be simple and efficient enough to be implemented on field-programmable gate arrays (FPGAs), allowing real-time processing. Pulse-shape analysis has already been used to perform, for example, α/γ discrimination in $LaBr_3$(Ce) crystals [12] and neutron/γ selection in liquid scintillators [13].

The purely statistical resolving time of a pair of detectors is given by $\delta t = \frac{\sigma}{\sqrt{n}}$ where n is the number of events and σ is the width parameter of the Gaussian function describing the distribution. Hence an experiment using detectors with twice worse time resolution will require 4 times the number of counts to achieve the same statistical precision. Therefore there is strong motivation to develop timing algorithms suitable for use with digital acquisition systems which have performances equivalent to, or better than, the best analogue pulse-processing electronics.

Improved timing resolution is also of interest for clinical PET applications, which would allow lower injected patient doses. Although

* Corresponding author.
E-mail address: garyssimpson99@gmail.com (G. Simpson).

https://doi.org/10.1016/j.nima.2019.05.015
Received 29 August 2018; Received in revised form 30 April 2019; Accepted 5 May 2019
Available online 9 May 2019

the γ-ray detectors used in PET applications are much smaller than the crystals used for nuclear excited-state lifetime measurements, equivalent pulse-processing techniques are used to extract timing information. Clinical PET time resolutions better than 100 ps would allow some of the artefacts affecting tomographic reconstruction to be removed for devices with partial angular coverage [14]. For resolutions of 10 ps time-consuming image reconstruction techniques would not be required, as true real-time 3-D image information would be available [14]. In the case of prompt-γ timing for particle therapy, transitions with energies typically in the range 3–6 MeV are measured, for which better time resolution is expected than at 511 keV [2].

With this in mind we have measured the time resolution of a pair of fast $LaBr_3$(Ce) scintillator detectors when applying four different digital algorithms to extract timing information. These algorithms were a leading-edge discrimination of the raw detector pulse and also following a cubic polynomial fit to the rising slope, a digital constant-fraction discriminator and an ideal-pulse autocovariance function. The first and third pulse-processing algorithms are equivalent to analogue fast-signal treatment schemes. These algorithms differ from other fast filters often implemented on commercial digital acquisitions systems for use with Ge detectors, such as trapezoidal ones. These fast-filters have the aim of distinguishing real low-energy signals from noise. Limited tests of these algorithms within the present work gave degraded timing performance in comparison with the ones used below, however this does not exclude that a well-tuned algorithm of this type, with its inherent noise filtering, may give improved results in the future. The experiments were performed with a digital oscilloscope running at a sampling frequency of 40 GS/s, with a 4 GHz bandwidth and 10-bit vertical resolution. The effect of varying the sampling frequency was also studied.

2. Experimental setup

The time resolution of $\gamma - \gamma$ coincidences detected in a pair of scintillator detectors was studied in order to determine pulse-processing algorithm performance. A pair of conical shaped $LaBr_3$(Ce) scintillator detectors were used to detect γ rays emitted from ^{60}Co and ^{152}Eu radioactive sources. The detectors were placed ~2.5 cm from the source and at 90° to each other, to minimize Compton scattering. The $LaBr_3$(Ce) crystals were 38 mm long and 38-mm wide at the base. Their exact dimensions are reported in [3]. These crystals were mounted on Hamamatsu R9779 photomultiplier tubes (PMTs). The anode output signal of the PMT base was connected directly to the oscilloscope and the dynode output was terminated with a 50-Ω resistor. The oscilloscope was a LeCroy HDO9404 model with 10-bit vertical resolution and a vertical range of 1 V. It ran at a sampling speed of 40 GS/s. Each digitized trace was 4096 samples (102.4 ns) long, enough to contain all of the $LaBr_3$(Ce) signal trace. The oscilloscope ran in an "AND" mode where traces were captured only if triggers on both signals fired within a time window of a few nanoseconds. The high voltage was set to ~-1100 V so that pulses with energies up to ~1.5 MeV could be recorded on the oscilloscope. This voltage is slightly lower than the −1200 V used in [3], which was found to be optimal with the same detectors. The limited vertical acceptance range of the oscilloscope (1 V) meant that the optimal voltage could not be used. However, in [15] the difference in resolution between $LaBr_3$(Ce) detectors operating at −1100 V and -1300 V was found to be ~15 ps. Hence the use of a slightly lower than optimal voltage is expected to result in only a small degradation in time resolution (<15 ps).

Data taken with a 264-kBq ^{60}Co source were used to find the best resolution of each algorithm at energies of ~1.2 MeV. This source first β^- decays and then emits a cascade of two γ rays of energy 1173.2- and 1332.5-keV. The halflife of the intermediate state is 0.7 ps, negligible compared to the time resolution of the γ-ray detectors. Some 3×10^5 coincident traces were captured.

A 27.0-kBq ^{152}Eu source was used to determine how the different algorithms perform for γ-ray transitions across a wider energy range. A total of 3.1×10^6 coincidence traces were recorded. Around 20 intense γ rays are emitted by this source, which form $\gamma - \gamma$ cascades distributed in two nuclei, ^{152}Gd and ^{152}Sm [16]. These cover an energy range of 121.8 to 1299.1 keV, however several lifetimes of the intermediate states are in the 100-ps-to-ns time range. Use of these cascades would add appreciable widths to time spectra and are unsuitable for this study. However the 344.3-keV transition is coincident with five transitions covering an energy range of 367.8–1299.1 keV. For four of these $\gamma - \gamma$ coincidences the intermediate state is the 344.3-keV one, with a lifetime of 46.7 ps [16]. The fifth one is the 367.8–344.3-keV coincidence which is part of a triple-γ cascade with a mean lifetime of 57.2 ps. Therefore for this set of $\gamma - \gamma$ cascades mean lifetimes of a similar ~50 ps are present, allowing a qualitative comparison of the performance of each algorithm as a function of the γ-ray energy coincident with a 344.3-keV transition. The performance of these algorithms at energies of around 511 keV is relevant to PET applications [17], though the crystals used in the current study are optimized for lifetime measurements of excited nuclear states.

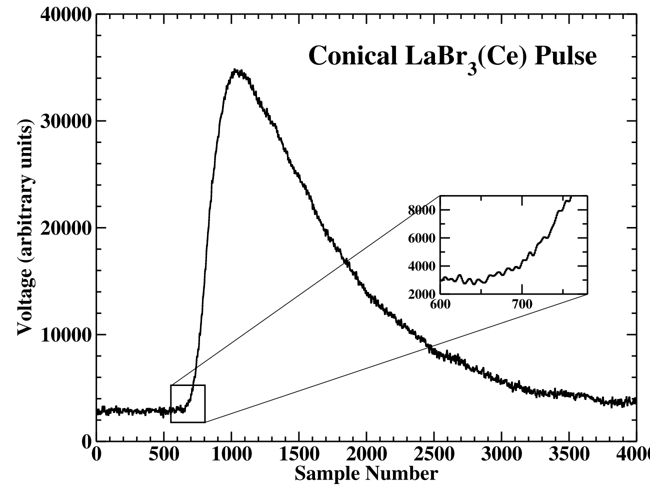

Fig. 1. Example of an anode pulse captured by the 40 GS/s oscilloscope. The data points shown are the ones analysed and these are the raw ones reflected about the x-axis, as explained in the text. The zoomed inset allows the noise present in the baseline and at the start of the rising pulse to be observed.

3. Algorithms and results with ^{60}Co

Before applying any timing algorithms the first procedure was to extract the average value of the pulse baseline. This quantity varies from pulse to pulse and was obtained simply by finding the average of the first 300 sample points. These all lie at times earlier that the first sample point registering the interaction of a γ ray, as can be seen in Fig. 1. This shows a typical anode pulse from one of the $LaBr_3$(Ce) detectors captured by the oscilloscope. The data points presented were reflected across the x-axis so that all values are positive. This was done to simplify algorithm implementation. The energy of the deposited γ-ray signal was found using a simple running integration algorithm, which sums all sample points found above the baseline. An energy resolution (FWHM) of 3.4(1)% was measured at 1332.5 keV, the same as reported in [9,10].

If the energies of both pulses were found to fall within ±20 keV of the individual photopeak energies of interest then timing algorithms were applied to the event. These algorithms are listed below. Examples of gated energy spectra measured using the ^{60}Co source are shown in Fig. 2. Here one observes only the other transition of the $\gamma - \gamma$ cascade and Compton background.

In order to quantify the timing performance of each algorithm when analysing $\gamma - \gamma$ events, differences between the trigger times of

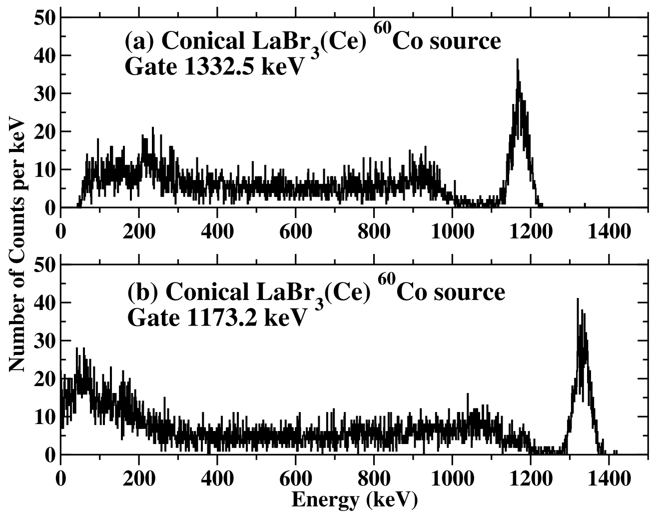

Fig. 2. Energy spectra obtained with the $LaBr_3$(Ce) detectors when energy gates are set on one transition and then the other of the cascade.

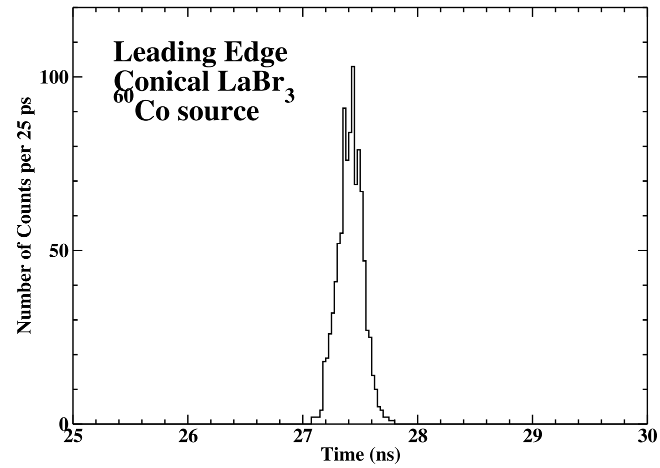

Fig. 3. Example time spectrum measured with the leading edge algorithm and a ^{60}Co source.

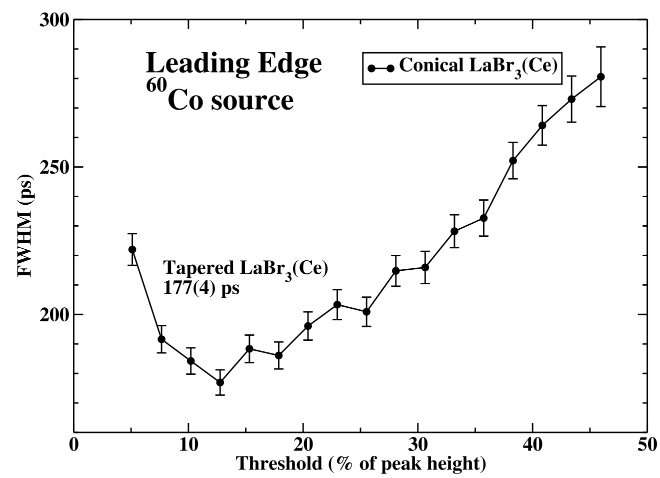

Fig. 4. Full width half maximum (FWHM) of time signals obtained with a leading-edge algorithm as a function of the threshold value for a single detector, de-convoluted from the measured distribution.

each detector were plotted. In all cases the full-width half-maximum (FWHM) value of the assumed Gaussian time distribution is used to define the resolution. As the detectors are essentially identical, then the measured FWHM can be divided by $\sqrt{2}$ to obtain the resolution of each individual detector, to a good approximation. This allows a comparison with results reported in the literature for each detector type, for example those of [3]. Identical γ-ray gates were set when processing the data with each algorithm.

3.1. Leading edge with a ^{60}Co source

The leading-edge algorithm produces a trigger-time marker when the pulse trace first crosses a set threshold. For the data taken with the ^{60}Co source, the FWHM was measured as a function of the threshold energy. Use of interpolation between the sample points did not improve the time resolution. This agrees with the conclusions of [8] for high sampling frequencies. There it was reasoned that the higher density of sampling points means that the difference between the actual detector pulse and a linear interpolation between any two sample points becomes negligible.

An example time spectrum obtained with the $LaBr_3$(Ce) detectors is shown in Fig. 3. The results obtained are shown in Fig. 4 where the change in FWHM is shown as a function of the threshold value. The maximum pulse height is around 35,000 (arbitrary units) and the best FWHM values are obtained with the threshold set at 10–20% of this maximum. A similar behaviour is found in analogue leading-edge modules and in previous studies using digital leading-edge algorithms (15%) [17]. One observes that there is a regular degradation of the FWHM with increasing threshold values. Threshold values below ∼5% of the pulse height produced spurious peaks due to noise. The best resolution obtained with this algorithm was 177(4) ps.

3.2. Cubic polynomial slope fit and leading edge with a ^{60}Co source

In order to remove any high-frequency noise contribution to the leading-edge algorithm, the rising slope of each trace was captured and fitted with a cubic polynomial function. This function was the lowest order polynomial found to accurately reproduce the rising edge of the detector pulses, in line with the results of [18]. A leading edge threshold was then applied to the fit function describing each individual pulse, producing a reference time. Fits were applied across rising slopes varying from 10%–90%, 5%–90%, 5%–50% and 5%–30% of the pulse peak height. The best results were obtained for fits over the range 5%–90% and 5%–50% of pulse height, where equivalent time resolutions, within errors [143(3) ps], were obtained. The threshold parameter was also varied until the smallest FHWM was found. A value close to the one in Section 3.1 was optimal. The results are shown in Fig. 5. One notes that it is possible to apply this algorithm with a lower threshold value than for the raw signals of Section 3.1, due to the absence of high-frequency noise on the fitted polynomial function.

The digital leading-edge algorithm of Section 3.1 and the cubic polynomial slope fit, followed by a leading edge trigger, used here trigger on signals in a very similar manner. A comparison of the results obtained by each allows an estimation of the influence of higher frequency noise harmonics on the signal time resolution, because high-frequency noise is smoothed out in the fit analysis. As noise contributions add in quadrature, then one obtains $FWHM_{highfreq}$=104(3) ps for the high-frequency noise component, a significant amount.

3.3. Constant fraction with a ^{60}Co source

The constant fraction (CFD) algorithm used in the analysis of the detector signals is the digital equivalent of the ones used in analogue modules. An input signal is duplicated, inverted and delayed. The original signal is then attenuated by a fraction f and the zero-crossing

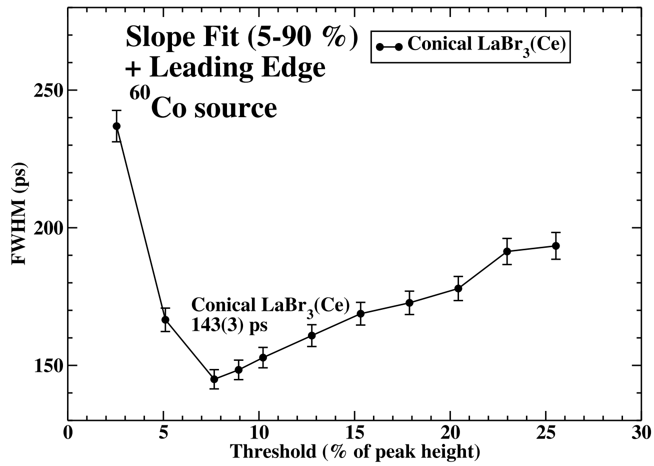

Fig. 5. Full width half maximum (FWHM) of time signals obtained with a cubic slope-fit algorithm as a function of the threshold value for a single detector, de-convoluted from the measured distribution.

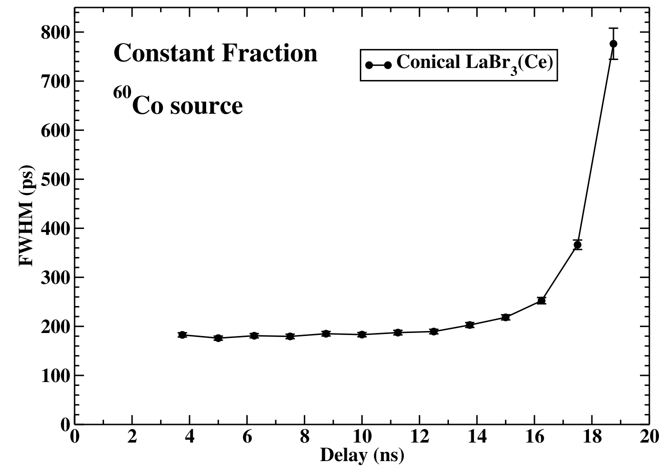

Fig. 7. Full width half maximum (FWHM) of a digital constant-fraction algorithm as a function of the delay time of the duplicated signal for a single detector, de-convoluted from the measured distribution. A fraction of f=0.18 was used.

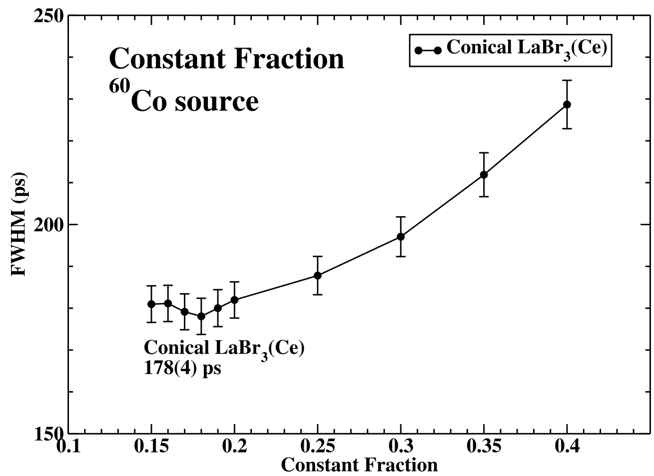

Fig. 6. Full width half maximum (FWHM) of a digital constant-fraction algorithm as a function of the fraction of the attenuated signal for a single detector, de-convoluted from the measured distribution. A delay of 6.25 ns was used.

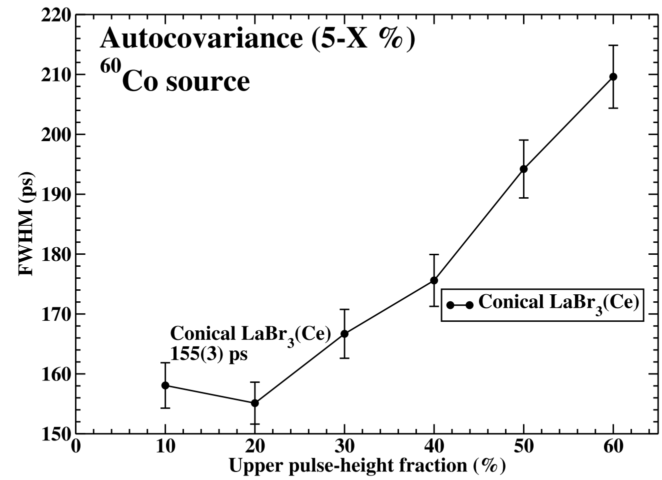

Fig. 8. Full width half maximum (FWHM) of a digital autocovariance algorithm as a function of upper limit of the peak signal voltage for a single detector, de-convoluted from the measured distribution.

of the sum of these two signals corresponds to the reference time. The CFD algorithm is written as

$$CFD[i] = f \times V[i] - V[i - delay] \quad (1)$$

where f is the fraction of the attenuated signal, $V[i]$ is the pulse height of the sample at bin number i and $delay$ is the time by which the duplicated signal is retarded [19]. This algorithm was tested over a range of values of f, from ∼0.2 to 0.4, corresponding to the ones used in analogue modules. Values of f below 0.15 could not be applied due to noise. The results are shown in Fig. 6. Similarly the $delay$ parameter was varied until an optimal result was obtained. The best delay values are close to the peak rise time, again in line with the settings of an analogue CFD. The performance of the algorithm is relatively insensitive to changes in delay times over a large range of values, as shown in Fig. 7. A time resolution of 178(4) ps was the best one obtained with this algorithm.

3.4. Autocovariance with averaged pulse-shapes with a ^{60}Co source

For each pair of applied energy gates pulses in each detector were summed and then averaged. This produced approximately "ideal" pulses, almost noise free, though still retaining any subtle systematic inflexions inherent to each detector pulse.

Once the set of average pulses had been obtained then each pulse in a given detector, falling within the range of the energy gate, was then compared to it. This was done by calculating the variance between the rising slope of a pulse of a given event and the average one, within the same height interval, using Welford's algorithm [20]. The event pulse was then shifted by one sample and the variance calculated again. Once the variance had been calculated across a set range of shifts, the minimum variance was obtained, allowing the "lag" between the individual pulse and the average one to be determined. The lag value can then be used to determine a trigger time. It is worth noting that this algorithm has no threshold dependence.

The vertical range over which the variance was calculated was changed and the optimal one was found to be 5%–20% of the pulse height, giving a resolution of 155(3) ps. This is shown in Fig. 8, where resolution is plotted as a function of analysed pulse height. Equivalent results were obtained when comparing 20 channels of the event pulse to the average one, once a low-energy threshold was crossed. This latter method is less computationally intensive.

The method described here is practically identical to the "Mean PMT pulse model" used by Aykac et al. to analyse pulses from LSO cyrstals [21]. We note that a procedure with a similar philosophy has been used for an entirely different γ-ray spectroscopy application. The

Table 1
Summary of best values of FWHM achieved for each algorithm with a ^{60}Co source and a 10-bit 40 GS/s oscilloscope.

Leading edge	Leading edge slope fit	CFD	Autocovariance
177(4) ps	143(3) ps	178(4) ps	155(3) ps

shapes of pulses recorded from the segmented outer contacts of 36-fold AGATA Ge detectors are compared to those found in a library of measured interactions [22]. This allows the interaction position of γ rays to be found with a precision of a few mm in a large-volume Ge detector.

3.5. ^{60}Co Source results summary and comparison with literature

A summary of the results obtained with each algorithm is shown in Table 1. As ∼1000 $\gamma-\gamma$ coincidences were analysed, then the statistical contribution to the error ($\frac{\sigma}{\sqrt{n}}$) is around 2 ps. These results can be compared to the time resolutions reported in the literature using analogue pulse-processing electronics. A study of the performance of conical $LaBr_3$(Ce) detectors, with the same dimensions as used here, reported a FWHM value of 110(3) ps with a ^{60}Co source [3]. The results obtained with the cubic polynomial slope fit are 30(1)% worse. In a recent study using a 16-bit 5 GS/s digitizer with the same $LaBr_3$(Ce) detectors a time resolution of 106(1) ps was reported, using the same type of radioactive source and a timing algorithm developed using machine learning [10]. This result surpasses all the ones obtained in the present work. In [8] a spline interpolation with a sinc function of the pulse rising slope using a 14-bit, 0.5 GS/s digitizer gave results equivalent to those reported using analogue electronics [3] for "1×1" $LaBr_3$(Ce) crystals [97 ps versus 98(2) ps]. This shows that a higher sampling frequency does not necessarily lead to improved time resolution if the vertical resolution is low and these points are discussed below.

4. Sampling frequency

The performance of each algorithm was tested as a function of sampling frequency, using the data taken with the ^{60}Co source. The results are shown in Fig. 9. Optimal parameters at sampling rates of 40 GS/s, reported in previous sections were used throughout. Unsurprisingly the best performance is found at a sampling frequency of 40 GS/s, though little degradation of the FWHM is seen at 20 GS/s. At sampling frequencies of 4 or 5 GS/s, the resolution is typically 30–60% worse. The results obtained in the present work differ from the conclusions of Aykac et al. [21] who studied the performance of small LSO detectors for PET applications. There they found that optimal digital algorithm performance was already attained at a sampling rate of 4 GS/s. Similarly Warburton and Henning [8] and Nakhostin et al. [10] were able to obtain results equivalent to the best ones achieved with analogue systems, though at lower frequencies of 0.5 and 4 GS/s using digitizers with 14 and 16 bits. This points towards vertical resolution being a more important parameter than sampling speed in the GS/s domain for $LaBr_3$(Ce) detectors. More formally the vertical resolution (number of bits) must be high enough that the quantization error is below the electronic noise of the signal [18].

5. ^{152}Eu data

The evolution of the peak FWHM as a function of energy, measured with the ^{152}Eu source is shown in Fig. 10. Here one gate was set on the 344.3-keV γ-decay of ^{152}Gd and the peak FWHM was measured when the second gate was set at other photopeak energies (367.8, 411.1, 778.9, 1089.7 and 1299.1 keV). There were around 1000 counts in each coincidence time spectrum. The 344.3–1089.7-keV data points were removed from the fit as they were found to be systematically higher

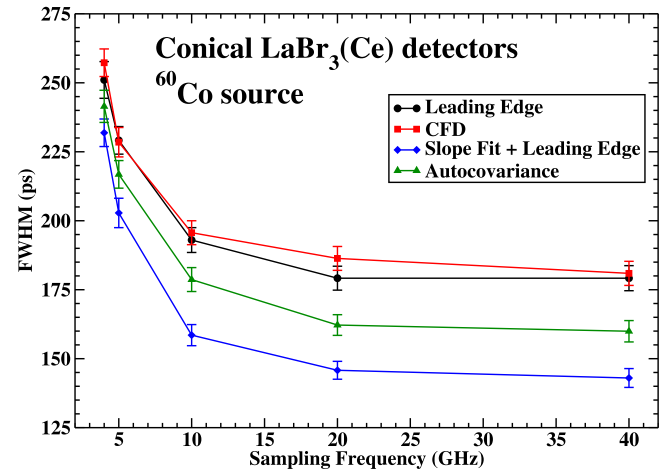

Fig. 9. Full width half maxima (FWHM) of time peaks extracted with different digital algorithms as a function of sampling frequency for a single detector, de-convoluted from the measured distribution.

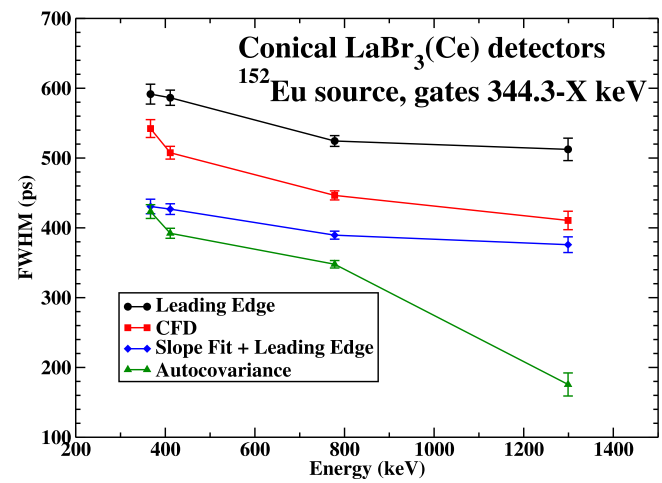

Fig. 10. Measured peak full width half maximum (FWHM) values as a function of transitions found in coincidence with the 344.3-keV γ ray emitted following the decay of a ^{152}Eu source.

than the trend lines, likely due to contamination with the 1085.9-keV transition in ^{152}Sm.

In Fig. 10 the autocovariance function is seen to have the best resolution across the range of energies studied. This energy range is typical of fast-timing experiments aiming to study the lifetimes of excited states in the 10s-of-ps to ns time range.

An important parameter in fast-timing measurements is the prompt-response difference (PRD) [6,7,16]. This function is used to determine the zero-time position as a function of energy and it depends on the settings of the analogue discriminator used. The "walk" of this zero-time position typically changes by a few hundred picoseconds over an energy range of 100 keV to 1.5 MeV. Uncertainties in the PRD generally limit the precision of high-statistics fast-timing measurements, hence the interest in obtaining PRD functions which are as flat as possible [23,24]. Despite the 3.1×10^6 coincident events recorded with the ^{152}Eu source there were insufficient statistics to reliably determine the PRDs of the all digital algorithms tested here.

6. Conclusion

The time resolutions obtained with four different timing algorithms have been measured with a pair of 38-mm long, 38-mm wide truncated-cone shaped $LaBr_3$(Ce) fast-timing detectors using a 10-bit, 40 GS/s oscilloscope. The time resolution obtained with a cubic polynomial slope fit leading-edge algorithm gave the best result with a ^{60}Co source [143(3) ps], though this is 30(1)% worse than values achieved using analogue pulse-processing electronics. The performance of the autocovariance function was slightly inferior [155(3) ps], but better than the leading edge [177(4) ps] and constant-fraction [178(4) ps] algorithms. The autocovariance function was found to have the best performance for coincidences in the energy range 344.3–1299.1-keV. This may be because the cubic polynomial slope fit algorithm used relies on a leading-edge threshold trigger, with settings optimized for ^{60}Co lines. The performance of this algorithm may therefore degrade when applied to lower-energy γ-rays. Reducing the sampling frequency to 20 GS/s was found to only slightly degrade the time resolution of these algorithms. The results obtained in the present work are a few tens-of-picoseconds worse than those obtained using a 16-bit, 5 GS/s digitizer module [106(1) ps] [10], demonstrating that high vertical resolution is more important than sampling speed in the GS/s domain when using these detectors.

Acknowledgements

O. Bourrion, G. Bosson and Ch. Vescovi of the LPSC Grenoble are thanked for helpful discussions. Financial support for this project was provided by NuPNET/IN2P3. The IKP Cologne, NIPNE Bucharest and the ILL Grenoble are thanked for the loan of equipment. The authors (DD, MLGM, SM and SC) acknowledge support from LabEx PRIMES (ANR-11-LABX-0063), INCa Physique-Cancer (CLaRyS-UFT project) and the FP7 MEDINET-ENSAR2 framework.

References

[1] H. Mach, R.L. Gill, M. Moszyński, Nucl. Instrum. Methods Phys. Res. A 280 (1989) 49–72.
[2] J. Krimmer, D. Dauvergne, J.M. Létang, E. Testa, Nucl. Instrum. Methods Phys. Res. A 878 (2018) 58–73.
[3] V. Vedia, M. Carmona-Gallardo, L.M. Fraile, H. Mach, J.M. Udías, Nucl. Instrum. Methods Phys. Res. A 857 (2017) 98–105.
[4] O.J. Roberts, A.M. Bruce, P.H. Regan, Zs. Podolyák, C.M. Townsley, J.F. Smith, K.F. Mulholland, A. Smith, Nucl. Instrum. Methods Phys. Res. A 748 (2014) 91–95.
[5] L. Fraile, et al., Technical design report for the DESPEC fast timing array, 2015.
[6] J.-M. Régis, et al., Nucl. Instrum. Methods Phys. Res. A 726 (2013) 191–202.
[7] J.-M. Régis, et al., Nucl. Instrum. Methods Phys. Res. A 763 (2014) 210–220.
[8] W.K. Warburton, W. Hennig, IEEE Trans. Nucl. Sci. 64 (2017) 2938–2950.
[9] M. Nakhostin, Z. Podolyak, P.H. Regan, J. Instrum. 9 (2014) C12049.
[10] V. Sánchez-Tembleque, V. Vedia, M. Carmona, L.M. Fraile, S. Ritt, J.M. Udías, in: IEEE Nuclear Science Symposium, Medical Imaging Conference and Room-Temperature Semiconductor Detector Workshop, 2016.
[11] F. Crespi, V. Vandone, S. Brambilla, F. Camera, B. Million, S. Riboldi, O. Wieland, Nucl. Instrum. Methods Phys. Res. A 620 (2010) 299–304.
[12] M. Zeng, J. Cang, Z. Zeng, X. Yue, J. Cheng, Y. Liu, H. Ma, J. Li, Nucl. Instrum. Methods Phys. Res. A 813 (2016) 56–61.
[13] M. Aspinall, B. DMellow, R. Mackin, M. Joyce, Z. Jarrah, A. Peyton, Nucl. Instrum. Methods Phys. Res. A 578 (2007) 261–266.
[14] P. Lecoq, IEEE Trans. Rad. Plasma Med. Sci. 1 (2017) 473–485.
[15] J.-M. Régis, et al., Nucl. Instrum. Methods Phys. Res. A 684 (2012) 36–45.
[16] J.-M. Régis, G. Pascovici, J. Jolie, M. Rudigier, Nucl. Instrum. Methods Phys. Res. A 622 (2010) 83–92.
[17] M. Ahmed, B. Camanzi, J. Matheson, Nucl. Instrum. Methods Phys. Res. A 695 (2012) 252–256.
[18] L. Bardelli, G. Poggi, M. Bini, G. Pasquali, N. Taccetti, Nucl. Instrum. Methods Phys. Res. A 521 (2004) 480–492.
[19] A. Fallu-Labruyere, H. Tan, W. Hennig, W. Warburton, Nucl. Instrum. Methods Phys. Res. A 579 (2007) 247–251.
[20] R.F. Ling, J. Amer. Statist. Assoc. 69 (1974) 859–866.
[21] M. Aykac, I. Hong, S. Cho, Nucl. Instrum. Methods Phys. Res. A 623 (2010) 1070–1081.
[22] S. Akkoyun, et al., Nucl. Instrum. Methods Phys. Res. A 668 (2012) 26–58.
[23] J.-M. Régis, et al., Nucl. Instrum. Methods Phys. Res. A 823 (2016) 72–82.
[24] J.-M. Régis, et al., Nucl. Instrum. Methods Phys. Res. A 897 (2018) 38–46.